

Comparison of the techniques pH indicator and optical microscopy for determination of carbonation depths on Portland cement, fly ash, slag and 3-powder concretes.

Abstract

The aim of this paper is to compare the information gained from determination of carbonation depths measured by pH indicator and optical microscopy for 4 samples naturally exposed in urban environment outside DTI for 8 years. Thymolphthalein was used as the pH indicator and the optical microscopy was performed on thin sections. The terminology proposed in (Revert, De Weerd et al. 2016) was used to characterize the carbonation depth and front. The carbonation depths determined by pH indicator and optical microscopy are in relatively good agreement when considering the impact of sampling.

Introduction

Carbonation induced corrosion is one degradation mechanism, which can cause premature deterioration of reinforced concrete structures. Carbonation is the process where hydration products containing calcium react with CO_2 to form calcium carbonate thereby lowering the pH of the pore solution and rendering steel depassivated. The rate of carbonation is influenced by the porosity, composition and humidity of concrete (Jacobsen, Sellevold et al. 2009). In addition to the hydration products, unhydrated phases such as alite and belite may carbonate (Papadakis, Vayenas et al. 1991).

(Bier 1986) found that the carbonation depths in well-cured samples containing fly ash or blast furnace slag can be a factor of 2 greater than when ordinary Portland cement is used (Bier 1986).

Carbonation can be either beneficial or detrimental to concrete. The compressive strength and density can increase, while the porosity and permeation properties can decrease due to the carbonation products consisting primarily of calcium carbonate taking up about 11.7% additional space than $\text{Ca}(\text{OH})_2$ (Russell 1999, Xu, Wang et al. 2011, Wang, Nanukuttan et al. 2017). Alternatively, the permeation properties may increase due to carbonation causing shrinkage of hydrated cement paste (Parrott and Hong 1991, Saeki 2004, Wang, Nanukuttan et al. 2017).

Several methods are available for determination of carbonation in concrete as described by (Revert, De Weerd et al. 2016). Methods include pH indicator, thermogravimetric analysis, Fourier-transformed infrared spectroscopy, X-ray diffraction, optical microscopy, scanning electron microscopy, mercury intrusion porosimetry, magic-angle spinning nuclear magnetic resonance spectroscopy, gammadensimetry and chemical analysis (Revert, De Weerd et al. 2016). In the present paper the techniques pH indicator and optical microscopy is utilized and compared.

The most common way to study carbonatization depth in concrete is to spray a solution containing a pH indicator. Traditionally Phenolphthalein has been used, but due to the carcinogenic classification of Phenolphthalein, Thymolphthalein is increasingly used instead. Thymolphthalein has the property to be blue above pH 9.3-10.5 and colorless below. The carbonation depth is thus detected by the depth in which the color change from blue to colorless.

By optical microscopy carbonation can be identified by X-polarized light as opaline and bright colors due to presence of calcite crystals (and absence of calcium hydroxide). This is a sharp contrast to the darker colors of the non-carbonated areas. By polarized light carbonation may be identified by

absence of un-hydrated cement grains. Finally, fluorescent mode can reveal changes in porosity due to carbonation if an un-carbonated reference is available and the w/c is sufficiently low (Jakobsen, Laugesen et al. 1999).

The aim of this paper is to compare the information gained from determination of carbonation depths measured by pH indicator and optical microscopy for 4 samples exposed at urban exposure outside of DTI for 8 years.

Experimental

Material

Four concrete elements differing in binder compositions (Table 1) were investigated for microstructural changes due to carbonation. After homogenization in pan mixer, the elements were cast in plywood molds lubricated with mold oil. The elements were demolded at an age corresponding to minimum 24 maturity hours. Immediately after demolding, the blocks were wrapped in plastic secured firmly with tape. Each block remained indoors until the block had reached minimum 14 maturity days, where after the blocks could be moved outside if required to control maturity gain. The exact maturity of the blocks was monitored closely using cast-in temperature sensors. The plastic was removed when the blocks reached a maturity of 28-42 days. The exposure environment was in average 8.8 °C with 412 ppm CO₂, 674 mm precipitation and 1447 hours of sunshine (Buis 2019, DMI 2020).

Table 1: Composition of concretes selected for optical microscopy (Poulsen, Sørensen et al. 2018)

Concrete ID:		A	C	F	K	
Powder composition wt%	Low alkali SR cement CEM I 42.5 N	CEM I 42.5 N	100	75	84	
	Slag cement	CEM III/B 42.5 N				100
	Fly ash	EN 450-1 N		25	12	
	Silica fume	50 %-wt slurry			4	
Concrete composition	Cement	kg/m ³	365	300	300	360
	Fly ash	kg/m ³		100	43	
	Silica fume, solid matter	kg/m ³			14	
	Water content	l/m ³	146	140	140	144
	Aggregate 0/2	kg/m ³	695	642	677	689
	Aggregate 4/8	kg/m ³	377	367	377	373
	Aggregate 8/16	kg/m ³	266	271	272	263
	Aggregate 16/22	kg/m ³	529	541	543	525
	Air entraining agent	kg/m ³	1.7	2.3	1.6	0.8
	Superplasticizer	kg/m ³	2.8	2.2	2.9	2.3
Eqv. w/c ratio	-	0.4	0.4	0.4	0.4	

Methods

At an age of 8 years cores were drilled using a 100 mm drill. The cores were cut through lengthwise and any surface water was blown away by pressurized air. For each core, one cut surface was immediately analyzed by pH indicator, whereas the other was impregnated with fluorescent epoxy within one hour after cutting to stop further carbonation and to prepare thin sections for optical microscopy.

pH indicator

A thymolphthalein solution was prepared by dissolving 0.1 g thymolphthalein in 20 g deionized water and 80 g of ethanol. The solution was sprayed on freshly cut surfaces and the depth of carbonation was measured as the depth of color change in 7 equally distributed points. Whenever this resulted in

a measurement point in an aggregate particle, the average carbonation depth between the two sides of the aggregate particles was used. From these 7 points $x_{c,avg}$ (average of 7 measurement points), $x_{c,max}$ (maximum measured carbonation depth excluding cracks) and $x_{c,crack}$ (carbonation depth along crack) was determined.

Optical microscopy

Microstructural changes were investigated using optical microscopy of thin sections. Thin sections were studied by an optical microscope Nikon Eclipse LV 100 POL. CH and CC crystals were observed using crossed polarized light. Carbonation depth was measured in 10 equally distributed lines across the width of the sample. Porosity changes due to carbonation were studied by comparing the intensity of the fluorescent light transmitted through the sample.

Terminology

The terminology proposed in (Revert, De Weerd et al. 2016) was used to characterize the carbonation depth and front. i.e. the carbonation depth $x_{c,i}$ is the distance at location i from the outer surface inwards to which a color change is observed on a freshly split sample sprayed with a pH indicator. The carbonation depth is described by the spatial variation:

- Average (\bar{x}_c)
- Median (\tilde{x}_c)
- Range (δ_x)

The carbonation front is the area/volume in which the measured property (e.g. pH) changes due to carbonation. See Figure 1 (Revert, De Weerd et al. 2016).

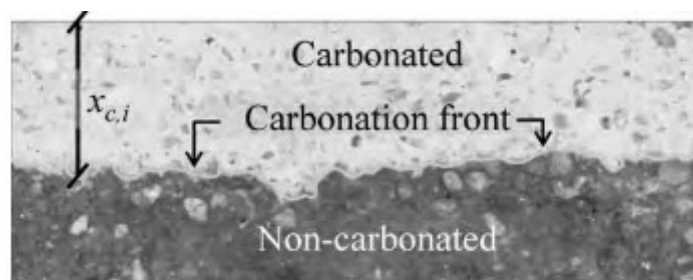


Figure 1: Used terminology to describe extent of carbonation (Revert, De Weerd et al. 2016).

Results

pH indicator

Carbonation was solely detected from the originally exposed surface and thus no carbonation occurred subsequent to drilling and extracting cores. Figure 2 shows sample A, C, F and K sprayed with thymolphthalein (exposed surface facing downwards).

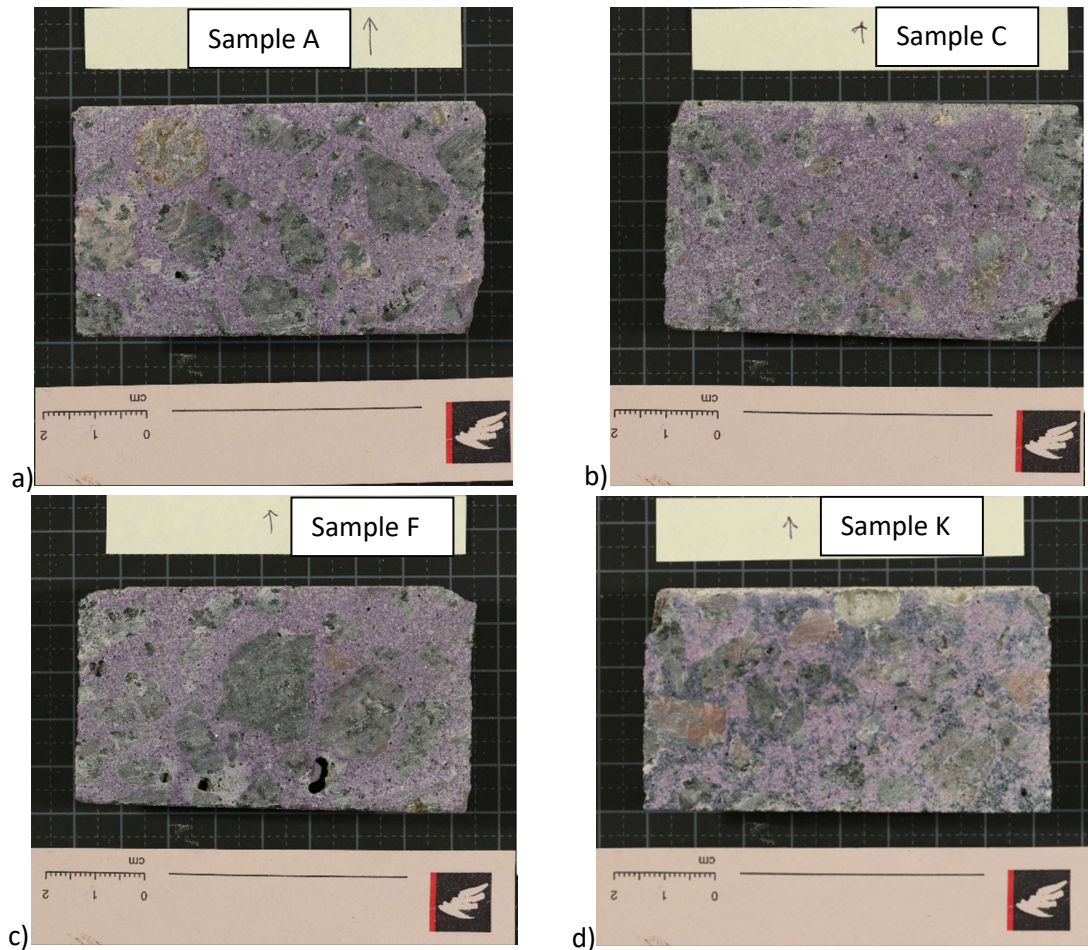


Figure 2: a) Sample A, b) Sample C, c) Sample F and d) Sample K sprayed with Thymolphthalein. Exposed surface pointing upwards.

Significantly larger carbonation depths are observed for concrete C and K than for A and F. K has an almost uniform carbonation front, whereas the carbonation front in concrete C varies across the width of the specimen. Figure 3 illustrates the spatial variation of carbonation depth in the 4 concretes determined by Thymolphthalein indicator.

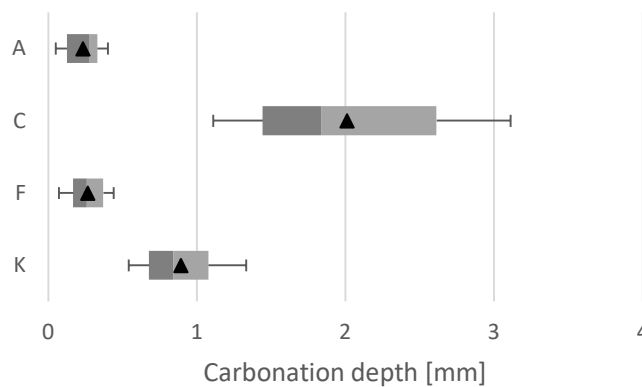


Figure 3: Spatial variation of carbonation depths determined using thymolphthalein. Boxes: values from 2nd and 3rd quartile and \bar{x}_c , whiskers: δ_x , black triangles: \bar{x}_c .

Optical microscopy

Concrete A

Figure 4C reveals a higher porosity in the surface region gradually increasing over about 500 μm . It is therefore not surprising carbonation is registered at the surface of concrete A after 8 years of exposure to an urban environment (Figure 4B). The air void structure is fair.

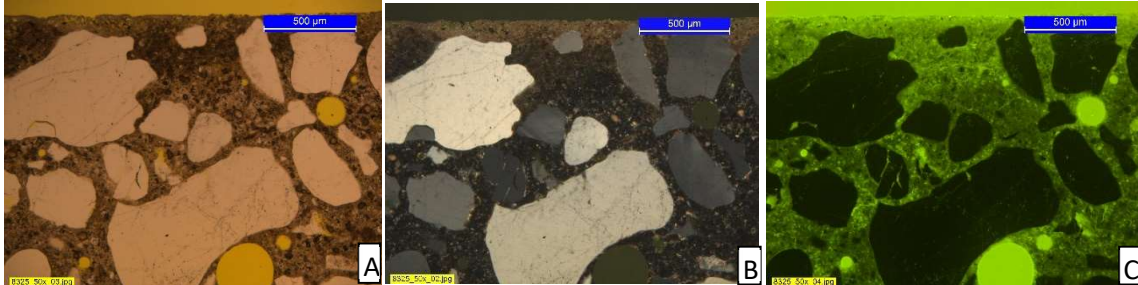


Figure 4: Picture of area in concrete A with representative carbonation in the three modes polarized light (A), X-polarized light (B) and Fluorescence (C). Concrete exposed for 8 years in urban environment. Exposed surface pointing upwards.

No cracks were observed in the surface and only few inside the thin section. However, Figure 5 shows a carbonated spot inside concrete A possibly originating from a crack extending from the surface out of the plane of the thin section. The diameter of the carbonated spot within the concrete is approximately twice that of the penetration depth from the surface, suggesting the carbonation could have occurred from an initial crack resulting from drying shrinkage.

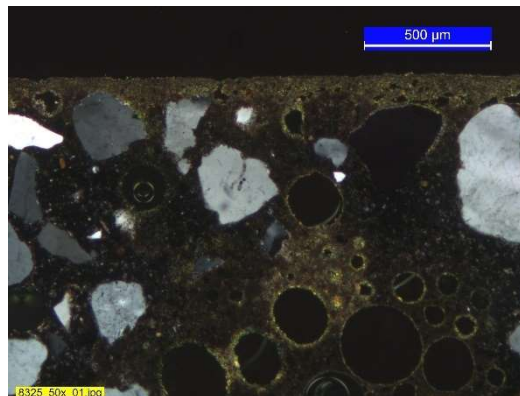


Figure 5: Carbonated area along crack inside of concrete A, which does not extend from the surface in the plane of the thin section. Exposed surface pointing upwards.

Concrete C

Figure 6B shows carbonation exceeding 1 mm in depth. Figure 6C reveals a uniform paste porosity, but an air void structure with air voids slightly agglomerating near aggregate particles. Contrary, a thin section prepared after 28 maturity days showed a weakly increasing porosity towards the surface thereby suggesting that carbonation following 8 years of urban exposure may have decreased the porosity of concrete C.

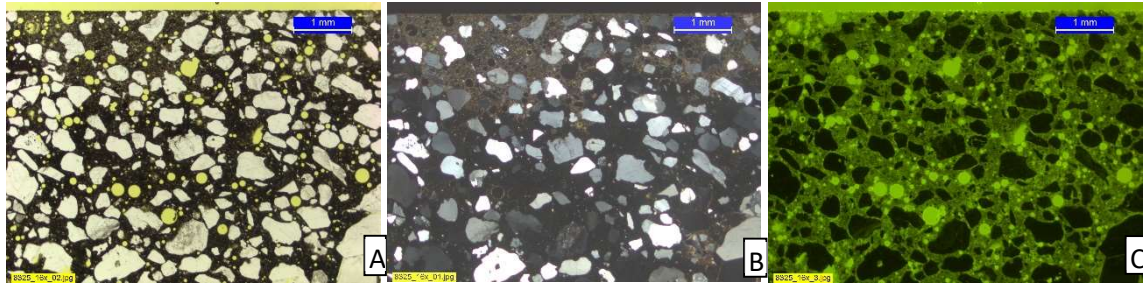


Figure 6: Picture of area in concrete C with representative carbonation in the three modes polarized light (A), X-polarized light (B) and Fluorescence (C). Concrete exposed for 8 years in urban environment. Exposed surface pointing upwards.

Concrete C studied after 8 years of urban exposure has two fine cracks. Figure 7 shows carbonation along a 11 mm long crack. The carbonated area along the crack is observed to be wide initially and end in a reservoir suggesting that the crack extends out of the plane of the thin section prior to returning. No cracks were detected on a thin section prepared after 28 maturity days, but the carbonation depth along the crack on Figure 7 suggests that this crack might have been there from an early stage.

The carbonation depth of concrete C has a relatively wide spatial distribution, which might be influenced by surface cracks either inside or outside the plane of this thin section.

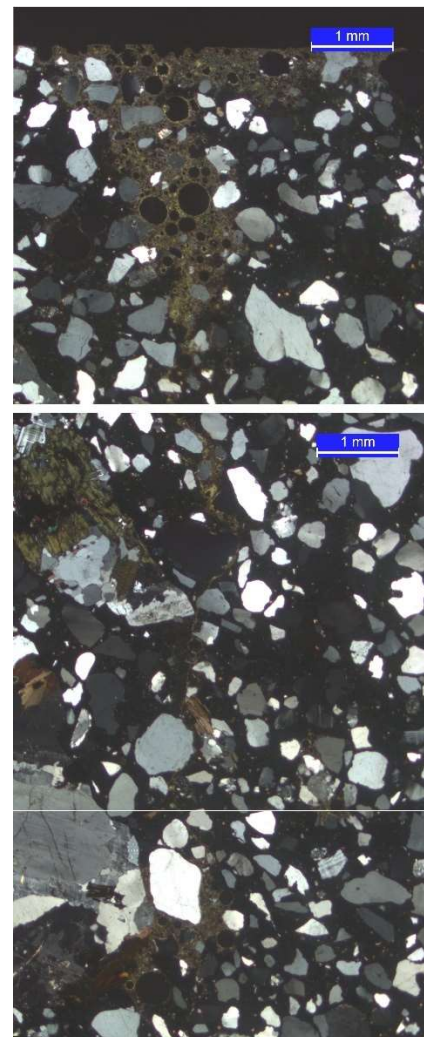


Figure 7: Large crack in concrete C. Exposed surface pointing upwards.

Concrete F

Figure 8C shows a uniform paste porosity increasing slightly towards the surface. The air void structure is poor with large clusters. Further cracks along aggregate and in the paste is observed. Despite the mentioned flaws, only a small carbonation depth is observed in concrete F (Figure 8B).

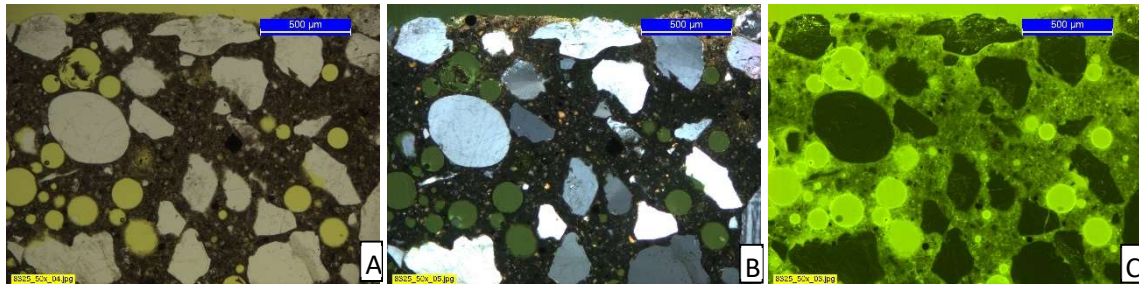


Figure 8: Picture of area in concrete F with representative carbonation in the three modes polarized light (A), X-polarized light (B) and Fluorescence (C). Concrete exposed for 8 years in urban environment. Exposed surface pointing upwards.

No cracks were observed in the surface. Very few paste and adhesion cracks were observed. Figure 9A and -B show additional examples of the poor air void structure in concrete F. The air is highly clustered around large aggregate particles. Figure 9C show carbonation in a large air void cluster near the surface of concrete F.

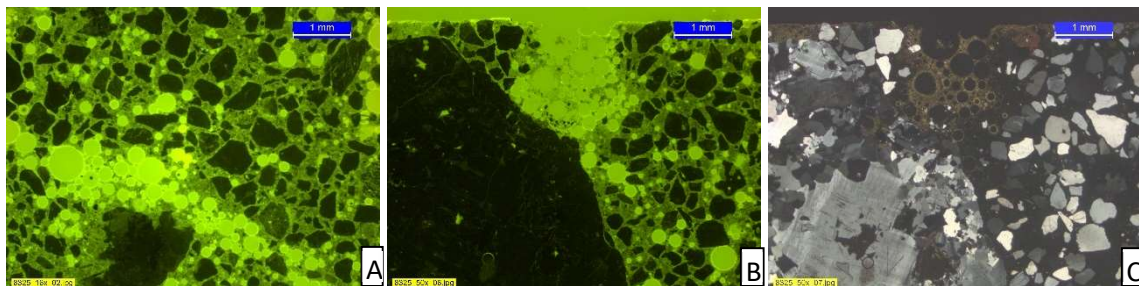


Figure 9: A) Poor air void structure in the interior of concrete F. B) Large air void cluster near the surface of concrete F. C) Carbonation in the large air void cluster shown on Figure 9B. Exposed surface pointing upwards.

Concrete K

Figure 10C shows a markedly higher porosity in the outer 1 mm of concrete K. The area of increased porosity observed on Figure 10C corresponds well with the carbonated area observed on Figure 10B. Judging from the area of concrete K shown on Figure 10 it might seem like the porosity is lower in the outer 0.5 mm than between 0.5-1mm. This feature is however not representative for the entire thin section and could be caused by a crack or air voids located in the third dimension in the depth 0.5-1mm. Generally, the air voids appear well-distributed.

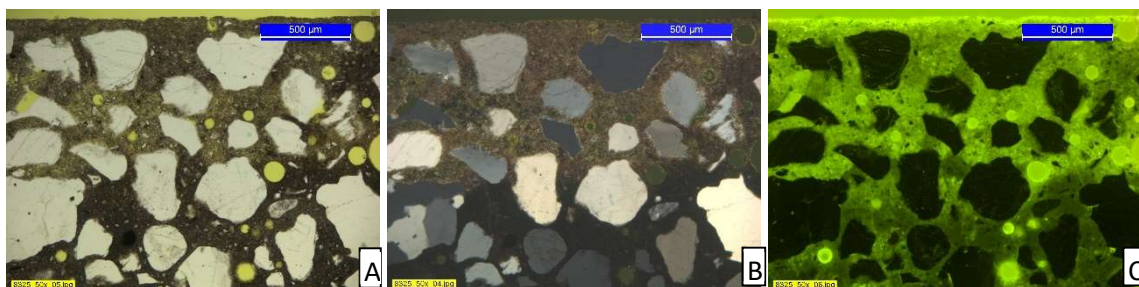


Figure 10: Picture of area in concrete K with representative carbonation in the three modes polarized light (A), X-polarized light (B) and Fluorescence (C). Concrete exposed for 8 years in urban environment. Exposed surface pointing upwards.

Figure 11A shows high porosity for concrete K after 28 maturity days extending through the entire thin section. By comparing Figure 11A and Figure 10C it is clear, that a significant densification of concrete K in the region behind the outer 1 mm has occurred within 8 years of exposure in urban environment. This densification occurred behind the carbonation front shown in Figure 10B.

Figure 11B shows adhesion cracks along aggregate particles of concrete K exposed in urban environment for 8 years.

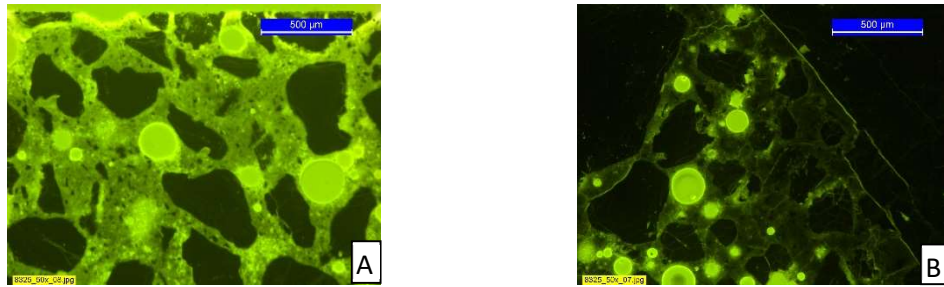


Figure 11: Porous surface of concrete K prior to exposure (28 maturity days) (A), adhesion cracks near aggregate particles of concrete K exposed for 8 years in urban environment (B). Exposed surface pointing upwards.

Figure 12A shows partly unhydrated cement grains in the interior of concrete K at 100x magnification. Figure 12B shows the outer ~0.5 mm of concrete K, where probably due to carbonation much less unhydrated cement grains are present.

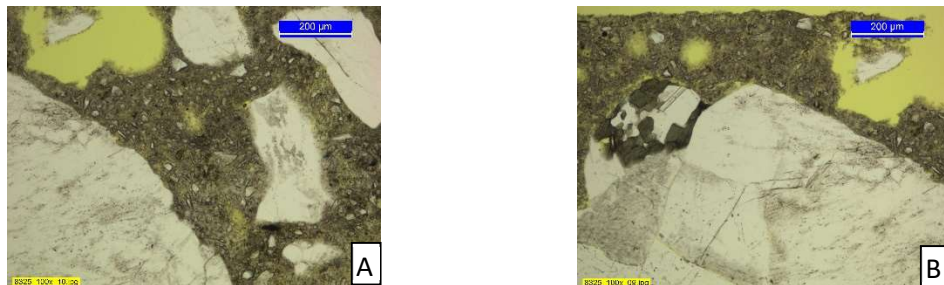


Figure 12: Partly unhydrated cement grains in the interior of concrete K detected in polarized light at 100x magnification (A), Absence of unhydrated cement grains due to carbonation detected in polarized light at 100x magnification (B). Exposed surface pointing upwards.

Summary of carbonation depths as measured by optical microscopy

Figure 13 illustrates the spatial variation of carbonation depths in the 4 concretes determined by Optical microscopy.

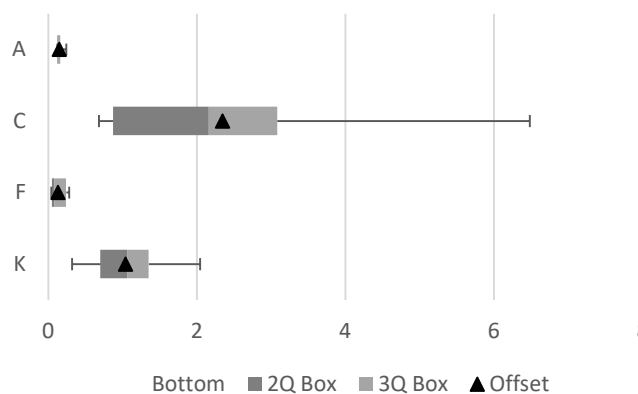


Figure 13: Spatial variation of carbonation depths determined using optical microscopy. Boxes: values from 2nd and 3rd quartile and \bar{x}_c , whiskers: δ_x , black triangles: \bar{x}_c .

Discussion

When comparing results of different techniques, the influence of sampling must be considered. The method pH indicator has a clear transition in color, whereas the method optical microscopy can be more subjective due to a possible wider transition from completely carbonated through partly carbonated to non-carbonated. The method pH indicator is convenient to apply, whereas optical microscopy provides additional information on e.g. porosity changes and cracks.

Figure 14 show a comparison between the spatial distribution of carbonation depth as determined by the pH indicator Thymolphthalein (THY) and optical microscopy (OM). It is seen, that considering the large range of determined carbonation depths, the average carbonation depths determined by THY and OM agree well. It is observed, that for the low carbonation depths of concrete A and F the carbonation depth is determined as lower by OM than by THY, while it is opposite for the larger carbonation depths.

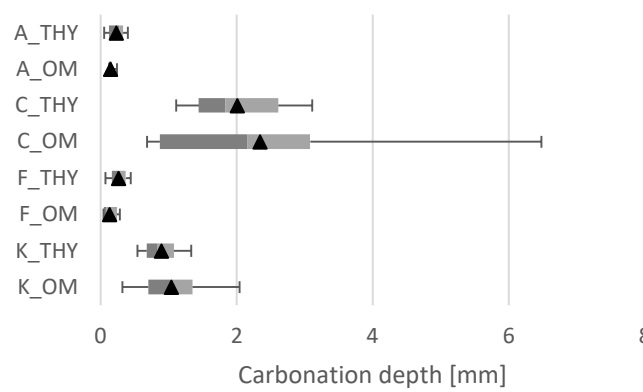


Figure 14: Comparison of spatial variation of carbonation depths determined using Thymolphthalein indicator (THY) and optical microscopy (OM). Boxes: values from 2nd and 3rd quartile and \tilde{x}_c , whiskers: δ_x , black triangles: \bar{x}_c .

No connection was found between the quality of the air void structure and the carbonation depths except from the special case depicted at Figure 9B+C. Between the four inspected concretes, concrete F had the poorest air void structure, while it together with concrete A by far has the lowest carbonation depth. However, it must be mentioned, that locally at the spot near the surface depicted at Figure 9B+C concrete F exhibited a carbonation depth of approximately 10 times the average carbonation depth of the sample. Also, it must be emphasized that the influence of the air void structure on carbonation depth is dependent on additional variables such as concrete compositions.

By optical microscopy carbonation along two fine cracks in concrete C was observed. This information is not available by simply spraying pH indicator, but it might be a contributing factor to the non-uniform carbonation front observed at Figure 2B.

Concrete A and F displayed only minor carbonation and their porosity remained largely unchanged over the exposure time. Concrete C, which carbonated most, showed a decrease of porosity in the carbonated zone. Finally, concrete K showed a large decrease in porosity, but behind the carbonation front. Based on these observations, a possible porosity decrease due to carbonation cannot be excluded.

Conclusion

The following conclusions were drawn:

- The method pH indicator is easy to apply, while optical microscopy provides additional information
- The carbonation depths determined by pH indicator and optical microscopy are in relatively good agreement when considering the impact of sampling.
- 5-11 times larger carbonation depths were found for concretes containing fly ash and slag compared to OPC based concrete.
- No connection was found between the quality of the air void structure and the carbonation depths.

References

- Bier, T. A. (1986). "Influence of type of cement and curing on carbonation progress and pore structure of hydrated cement pastes." MRS Online Proceedings Library Archive **85**.
- Buis, A. (2019). "The Atmosphere: Getting a Handle on Carbon Dioxide." Retrieved 03-01-2020, 2020, from <https://climate.nasa.gov/news/2915/the-atmosphere-getting-a-handle-on-carbon-dioxide/>.
- DMI (2020). "Danish meteorological institute." Retrieved 03-01-2020, 2020, from <https://www.dmi.dk/vejarkiv/>.
- Jacobsen, S., et al. (2009). TKT 4215 Concrete Technology 1, Department of Structural Engineering NTNU.
- Jakobsen, U., et al. (1999). "Determination of water-cement ratio in hardened concrete by optical fluorescence microscopy." Special Publication **191**: 27-42.
- Papadakis, V. G., et al. (1991). "Fundamental modeling and experimental investigation of concrete carbonation." Materials Journal **88**(4): 363-373.
- Parrott, L. and C. Z. Hong (1991). "Some factors influencing air permeation measurements in cover concrete." Materials and Structures **24**(6): 403-408.
- Poulsen, S. L., et al. (2018). Chloride ingress in concrete blocks at the Rødbyhavn marine exposure site - Status after 5 years. 4th International Conference on Service Life Design for Infrastructures (SLD4). Delft, The Netherlands: 192-203.
- Revert, A. B., et al. (2016). "Carbonation Characterization of Mortar with Portland Cement and Fly Ash, Comparison of Techniques." Nordic Concrete: 60.
- Russell, D. P. (1999). Influence of environmental conditions and material properties on carbonation in concrete, Queen's University of Belfast.
- Saeki, T. (2004). Effect of carbonation on chloride penetration in concrete. Third International RILEM Workshop on Testing and Modelling Chloride Ingress into Concrete, RILEM Publications SARL.
- Wang, Y., et al. (2017). "Influence of combined carbonation and chloride ingress regimes on rate of ingress and redistribution of chlorides in concretes." Construction and Building Materials **140**: 173-183.
- Xu, C., et al. (2011). "Interaction effect of chloride attack and carbonization in concrete." Journal of Building Materials **14**(3): 376-380.